Low Mach number simulation of a loaded standing-wave thermoacoustic engine

Lin Ma, Catherine Weisman, Diana Baltean Carlès, Patrick Le Quéré, Luc Bauwens

ACOUSTICS 2012

Low Mach number simulation of a loaded standing-wave thermoacoustic engine

L. Ma[a], C. I. Weisman[a], D. G. Baltean Carlès[a], P. Le Quéré[b] and L. Bauwens[c]

[a]UPMC - LIMSI, 4 Place Jussieu, 75252 Paris Cedex 05, France
[b]LIMSI, LIMSI - UPR3251, 91403 Orsay Cedex, France
[c]University of Calgary, Dept of Mechanical and Manufacturing Eng., Calgary, Canada AB T2N 1N4
malin@limsi.fr

Numerical simulations of a loaded standing-wave thermoacoustic engine are performed using a low Mach number model. This work uses a simplified model based on coupling the nonlinear flow and heat exchange in the heat exchangers and the stack with a linear acoustic model of the resonator and load. The two-dimensional unsteady numerical solution in the heat exchangers and stack region shows the amplification process until saturation is obtained. The influence of the load model on the wave saturation is studied, yielding a specific load range for saturation at levels comparable with experiments. In order to investigate the energy conversion within the standing-wave thermoacoustic engine, the acoustic power developed is calculated and the efficiency is estimated.

1 Introduction

A thermoacoustic engine is a device absorbing heat at the hot heat exchanger and releasing heat at the cold heat exchanger while producing acoustic work as an output. Such a device always requires adequate coupling with the load in order to achieve proper functionning.

A simplified model of a linear thermoacoustic engine consists of a stack of horizontal plates placed between two heat exchangers in a long tube ending at a dead end on one side and loaded on the other side. If the heat exchangers maintain a sufficiently large temperature gradient across the stack, work is produced through the combination of pressure fluctuation and oscillating heat exchange in the boundary layers along the plates [1, 2, 3]. There are few existing numerical simulations of such engines [4, 5].

In the present study, the engine is split into two different regions, the resonators and the active cell, comprising the heat exchangers and stack. The flow in the resonators is described by a standard linear one-dimensional acoustic model, and the active cell is investigated numerically using a two-dimensional Low Mach number model. An asymptotic analysis is used to couple the two regions. Details on this analysis can be found in [6, 7].

Numerical simulations using this approach show that depending on the load description and value, the engine can or cannot start. Also, the range of load values leading to saturation at pressure and velocity levels comparable with experiments is very narrow. An analytical approach considering the active cell as a source of volume inside a one dimensional linear acoustic wave guide shows the range of load values that should yield amplification of a given acoustic mode, and/or saturation at maximum acoustic power output. Simulations showed that for the load values corresponding to saturation at maximum power, the engine does not start. A numerical approach is then used to find the appropriate load values.

After a brief review of the model, the influence of the load model on the periodic operation of the engine will be discussed, using an analytical approach and a numerical approach. The simulation results will then be presented and discussed, showing for a given configuration, the specific load range for saturation at levels comparable with experiments. Finally, estimates of the acoustic power developed and of the engine efficiency will be shown and discussed.

2 Numerical model description

The geometry consists of a long tube with length L_{res}, within which an active cell with characteristic (stack) length L_{stack} is placed at a distance L_L from the left end. The active cell consists of a stack of horizontal plates placed between two heat exchangers also made of horizontal plates, having the same periodicity so that the simulation can be reduced to a domain consisting of two half-plates plus the gap between them, and a consistent fraction of the resonator cross-section. The geometry of the entire resonator and of the active cell are shown in Figure 1, as well as the corresponding dimensionless coordinate systems $\hat{x}$ and (x, y), using reference length L_{res} in the resonator and L_{stack} in the active cell. One resonator end, located at $\hat{x} = -l_L$ is closed, while the second consists of a load reduced to an impedance at a fixed location $\hat{x} = l_R$.

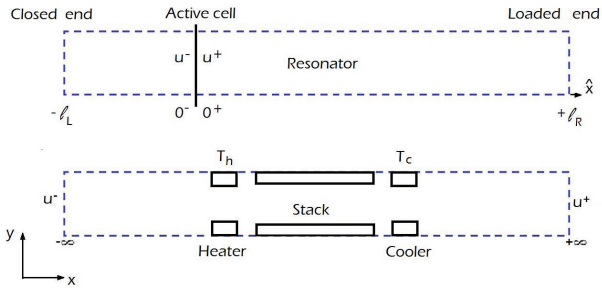

Figure 1: Geometry of linear acoustic system (top) and of active cell geometry (bottom).

The low Mach number model is obtained with a perturbation asymptotic method, described in detail in [6, 7]. The key scaling assumptions made is that at the stationary regime, velocities are small compared with the speed of sound, and that they span a length of the order of the length of the stack. Then since for an acoustic resonance, the resonator length is of the order of the speed of sound times the period, while the stack length is of the order of the velocity times the period, the ratio between the stack length L_{stack} and the resonator length L_{res} equals the reference Mach number M. Assuming a time scale of the order of the period, flow in the resonator is characterized by a linear acoustic problem. Flow in the active cell is described by a dynamically incompressible model, with order M^2 pressure gradients superimposed to spatially uniform pressure. In the solid stack plates the heat conduction equation is used.

At the solid boundaries, continuity of temperature and heat flux and no slip condition are imposed. Temperature is fixed in the heat exchangers, $T = T_c$ on the cooler plates, $T = T_h$ on the heater plates. The boundaries of the active cell are considered adiabatic.

Without loss of generality, acoustics in the two parts of the resonator can be expressed as a pair of plane traveling waves that move respectively left and right at the speed of sound. At tube ends, the boundary conditions result in a relationship that determines the outgoing wave as a function of the incoming wave. In the current context, this model reduces resonator acoustics to boundary conditions, on both sides of the active cell, relating order M pressure and velocity to their values at a previous time equal to the round trip time between the active cell location and the respective end

at the respective speed of sound.

Matching these two solutions in the standard way provides appropriate boundary conditions to the flow inside the active cell, depending of the impedance value at the load end. From the standpoint of resonator acoustics, the active cell is transparent to pressure but provides a source of volume.

The problem in the active cell is solved numerically using a finite volume code developed at LIMSI [6]. Diffusion is dealt with implicitly while advection is explicit. Schemes are second-order accurate in space and time. A fractional time step projection method adapted for variable density is used to enforce continuity. Both the ADI and GMRES algorithms have been tested to solve the Helmholtz equation for temperature and velocities. A multigrid algorithm determines the pressure correction. Solution of the coupled equations providing velocity boundary conditions from resonator acoustic are appropriately integrated in the solution sequence. An extensive validation of the current implementation was performed with satisfactory results [8]. Initial conditions considered fluid at rest and temperature profiles obtained numerically, corresponding to steady conduction in the walls and in fluid at rest. Simulations are performed for a fixed load. The load influence on the periodic operation of the engine is analyzed by varying the impedance value representing the load.

3 Analytical approach

In this section an analytical approach is developed to estimate the range of load values that should yield amplification of a given acoustic mode, and/or saturation at maximum acoustic power output. The resonator is considered to be a one dimensional linear acoustic wave guide, with single and unknown angular frequency ω. In accordance with the previous section, the active thermoacoustic cell is considered to act as a point source of volume associated to an imposed discontinuity in temperature, the acoustic pressure remaining unchanged between the entrance and exit of the active cell.

As shown in Figure 1 (top), the tube extends from $\hat{x} = -l_L$ to $\hat{x} = l_R$. The horizontal velocity u and the acoustic pressure p', solutions of the dimensionless linear acoustic equations can then be written on each side of the active cell in complex forms.

On the left (hot) side of the active cell, the dimensionless speed of sound is $a_L = \sqrt{T_h}$. The left end being closed, the corresponding boundary condition is $u(\hat{x} = -l_L) = 0$. The wave is a standing wave, with $\pi/2$ temporal phase shift between u and p'. The velocity amplitude on this left side of the active cell is called U.

The active cell, modeled as a point source in this description, is located at $\hat{x} = 0$, and the thermoacoustic effect is assumed to create a source of volume, which, unlike in the previous section, is not solved for explicitly. If $u^+ = u(0^-)$ and $u^- = u(0^+)$ denote the horizontal velocities at the left and right of the active cell respectively, then $u^+ = u^- + \Delta u$, in which Δu results from the thermoacoustic effect. It is characterized by a complex amplitude V, which can be defined such that if for example V is real, Δu is in phase with pressure.

The speed of sound on the right of the active cell is $a_R = \sqrt{T_c}$. The horizontal velocity u and the acoustic pressure p' can also be written on that side of the active cell in complex forms. At the right end, $\hat{x} = l_R$, there is a load characterized by the relationship $p' = fu$, with f complex. If f is assumed to be real, a purely dissipative load is considered.

Calling the temperature ratio $\alpha = a_L^2/a_R^2 = T_h/T_c$, the dispersion relation can be obtained is the following form:

$$-1 + \sqrt{\alpha}\tan\frac{\omega l_L}{a_L}\tan\frac{\omega l_R}{a_R} + \frac{iV}{U}\sqrt{\alpha}\tan\frac{\omega l_R}{a_R} = \frac{fa_R}{\gamma}\left(i\sqrt{\alpha}\tan\frac{\omega l_L}{a_L} - \frac{V}{U}\sqrt{\alpha} + i\tan\frac{\omega l_R}{a_R}\right) \quad (1)$$

This dispersion relation is complex. If ω is a complex number, with non zero imaginary part, then there is a nonzero growth rate. If the imaginary part of ω is negative, then the mode will be amplified. Otherwise, it will decay in time.

In the following, the specific situation of steady state (saturation) is discussed. Therefore focus is on ω real.

The complex velocity amplitude V of Δu can be rewritten as $V = U(v + iw)$, with only v contributing to work. In the case of ω real, assuming f is real, and introducing the symbol $\phi = fa_R/\gamma$, the dispersion relation (1) can be rewritten and separated into real and imaginary equations:

$$-1 + \sqrt{\alpha}\tan\frac{\omega l_L}{a_L}\tan\frac{\omega l_R}{a_R} - w\sqrt{\alpha}\tan\frac{\omega l_R}{a_R} = -v\phi\sqrt{\alpha} \quad (2)$$

$$v\sqrt{\alpha}\tan\frac{\omega l_R}{a_R} = \phi\sqrt{\alpha}\tan\frac{\omega l_L}{a_L} - w\phi\sqrt{\alpha} + \phi\tan\frac{\omega l_R}{a_R} \quad (3)$$

These two equations can be combined to eliminate w. If a new notation is introduced, $K = \tan^2\omega l_R/a_R$, one obtains that:

$$v = \frac{\phi(1+K)}{\sqrt{\alpha}(K+\phi^2)} \quad (4)$$

It can be shown that v is a monotonically increasing function of K for $\phi > 1$, and decreasing otherwise. At fixed K, however, v can be shown to be maximum when $\phi = \tan\frac{\omega l_R}{a_R}$, with value $v_{max} = (1+\phi^2)/(2\sqrt{\alpha}\phi)$ which is minimum when $\phi = 1$. If K (or ω) is known, one can then predict the value of ϕ (and that of load f) leading to the maximum value of v and to maximum acoustic power. This method gives an estimate of the load value f that would lead to maximum efficiency. However, the numerical solution being unsteady, the value of the angular frequency is unknown. Also, there is no reason why the solution should only be a single-frequency solution. Therefore, the unsteady numerical solution will be used to estimate which is the most unstable mode and the corresponding value of ω, before using the simple analytical approach just described.

4 Results and discussions

Numerical simulations were carried out for two cases of existing experimental academic thermoacoustic engines [6, 9], with a "short" thermoacoustic active cell inserted in a long resonator tube closed at both ends. Both of these experimental engines can be modeled using the simplified device introduced in Figure 1, by assuming lossless acoustics in the resonators and concentrating all dissipation at the loaded end.

In both cases the working fluid is helium, and the cold temperature (reference temperature) is $293K$. Both experimental configurations differ on their dimensions (resonator length, stack length, distance between the left end and the

active cell, plate spacing H) and on the conditions of the experiments (mean pressure, temperature difference) as summarized in Table 1.

Table 1: Geometry and conditions of experimental devices

Case	L_{res}	L_{stack}	L_L	H	p_0	ΔT
	(m)	(cm)	(m)	(mm)	(bar)	(K)
1	7.57	15	0.68	0.97	10	59
2	1.11	3.5	0.14	1.06	4.4	262

The numerical simulations were carried out using a regular two-dimensional mesh of the active cell (2048×32 grid points). Numerical studies were conducted on the one hand for the description of the initial amplification [6, 8], and on the other hand for the description of the transition from rest to periodic saturated operation. In the latter, the value of the load had to the adjusted. Simulation of an entire transition could be extremely long. The time step was adjusted in order to satisfy the stability conditions, so that there were 200 (beginning of simulation) to 2000 (end of simulation) time steps per acoustic reference period.

4.1 Analysis of the coupling between the engine and the load

In this section, the coupling between the load and the engine is analyzed in detail. Focus is on determining the possible values f of the load leading to saturation and periodic operation of the engine. One natural strategy is to simulate the transition from rest for several values of the load. For very high values of f, the initial amplification is very fast and amplitudes of acoustic pressure and velocities grow very quickly beyond realistic values. As the load value is lowered, the amplification takes longer to grow. For a certain value of f (depending on the case), the trend switches direction and as load is lowered further, the amplification takes place earlier. This is consistent with the existence of a value of the load that maximizes the power developed by the engine. Indeed, power becomes zero for both an infinite and a zero impedance, hence existence of a maximum for an intermediate value. It is clear that the power absorbed by the load reduces the power available for amplitude growth. For very low impedance, it can be shown that the frequency doubles. This is consistent with a zero impedance representing an open end, which leads to resonant modes with a frequency double than that for a closed end in straight tubes with uniform temperature.

By trial and error, a value of f leading to periodic operation can be found for the experimental case 1, equal to $f = 90$, the corresponding amplification of the acoustic pressure at the active cell location being shown in Figure 2. The entire simulation takes about 100 hours CPU time on a NEC SX8, mostly due to the last 10% of simulation, when amplitudes are high. This procedure is not efficient, and therefore other methods are experimented, described below.

According to the previous section, for a given acoustic mode corresponding to the angular frequency ω, it is possible to correlate the value of the load f and the value of v, characterizing the thermoacoustic effect as expressed in Eq. (4). At the end of the simulation of Figure 2 (top), a detail of the time signal shows (bottom of Figure 2) that the dimensionless period is close to $7.5ms$, meaning that the operating mode is close to the first harmonic (the acoustic reference period, based on the empty tube filled with helium at cold temperature being $15ms$).

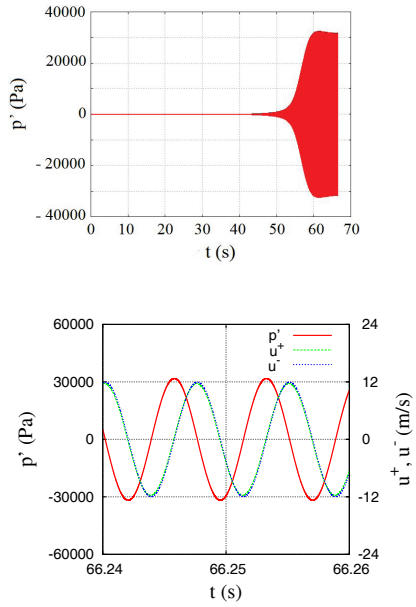

Figure 2: (top): acoustic pressure $p'(t)$, case 1, $f = 90$, with initial conduction temperature distribution and initial random noise.
(bottom): detail at the end of simulation of acoustic pressure $p'(t)$, left velocity u^-, right velocity u^+.

Therefore, v as a function of f was plotted (Figure 3) from Eq. (4) with the properties of the experimental case 1 and $\omega = 2\pi$. It shows that v is maximum for $f \approx 1.015$. If this value of f is imposed, the simulation shows that the engine does not start. The initially imposed small amplification dies out. As discussed in the previous section, Eq. (4) corresponds to the specific case of ω real, or steady operation. The study of cases where ω is complex, necessary for the amplification phase, should lead to a better estimate of f, and will be the object of future work.

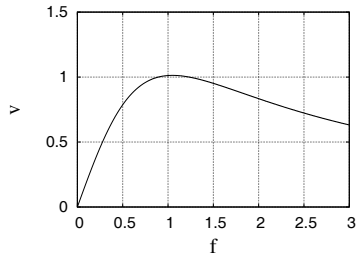

Figure 3: v as a function of f, case 1, with $w \approx 2\pi$ (first harmonic mode), $l_R \approx 0.91$, $a_R = 1$ and $\alpha = 1.2$.

Another numerical approach is also experimented, based on varying the value of the load f during the unsteady simulation. The initial value of f is chosen so that there is a clear instability and the wave is amplified. Then the value of f is lowered until a saturation is obtained, the simulation with a given value of f being discontinued as soon as the levels of amplification become to large. In this approach, the simula-

tion time has no physical meaning, but a value of f leading to saturation at levels (of acoustic pressure and velocities) comparable with experiments can be obtained in a much faster way (total CPU time of about 10 hours). One example of this approach is plotted on Figure 4 for the experimental case 2.

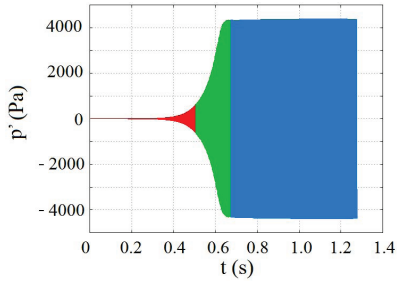

Figure 4: Acoustic pressure $p'(t)$, case 2, $f = 65$ (red), eight values of $f = 60, 55, 50, 45, 40, 39, 38$ (green), $f = 37.5$ (blue), with initial temperature linear between heat exchangers and initial random noise.

The numerical simulations for case 2 have shown that it is the fundamental mode (corresponding to an angular frequency $\omega \approx \pi$) that is most unstable. The analytical approach analogous to the one previously described for case 1 showed that the maximum value of ν corresponds to $f \approx 0.8$, for which again the engine does not start. The value found numerically for f is $f \approx 37.5$, which is much larger than the estimated "optimum" value. For this value of f, the analytical approach predicts a value of $\nu = 0.05$ which is much smaller than the optimum value of 0.9.

Having obtained one value of f leading to saturation at levels comparable with experiments, it is then interesting to assess the range of values of f leading to other saturation levels. In order to do this, the value of f was manually changed in the numerical simulations, starting from a saturated situation. For example in case 1, results were obtained from changing the value of the load from 90 to 80, from 90 to 85, and from 90 to 89. The transition from one value of f to the next takes a hundred of periods to stabilize. The choices $f = 89$ and $f = 85$ lead to new saturated situations, but the choice $f = 80$ leads to a wave decaying to zero. The range of values of f leading to observable periodic saturated operation is therefore narrow around $f = 90$.

Another possible approach, which has not been tested yet, would be to impose the analytical "optimum" value f, and impose a greater temperature difference between the heat exchangers in order to start the engine. Then the temperature difference could be lowered to experimental values.

In conclusion, finding the appropriate value of the load numerically is a CPU time consuming task, which can be shorten with appropriate use of analytical approaches such as that developed in Section 3. Other load models can also be tested, for example a model allowing for a given phase shift between acoustic pressure and velocity at the load end.

4.2 Analysis of periodic regime

Once saturation is obtained, the numerical solution can be analyzed in several ways. The harmonic content of the wave is one output of the unsteady simulation. The time signals of pressure and velocity at given points can be analyzed. For example, Figures 2 (bottom) and 5 show for cases 1 and 2 respectively, the time history of acoustic pressure at the active cell location, and of the velocities at the entrance and the exit of the active cell (corresponding to points $\hat{x} = 0^+$ and $\hat{x} = 0^-$ in the resonator coordinate system). As mentioned in the previous section, in case 1, the selected frequency for the periodic regime (Figure 2) is close to that of the first harmonic mode, and the phase shift between pressure and velocity are out of phase by almost $\pi/2$, which is consistent with a standing wave engine. The active cell creates small amplitude and phase modifications on the velocity between the entrance u^- and the exit u^+. Similar comments can be formulated for the periodic regime observed in case 2 (Figure 5), but in this case, the selected frequency for the periodic regime is close to that of the fundamental mode of the empty resonator filled with cold temperature gas.

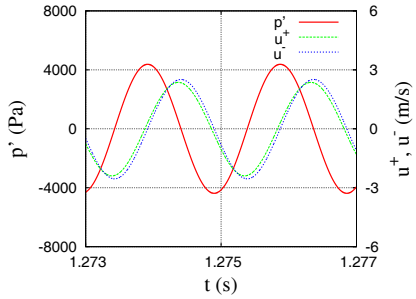

Figure 5: Detail (periodic regime) of acoustic pressure $p'(t)$ in case 2, left velocity u^-, right velocity u^+. $f = 37.5$, with initial temperature linear between heat exchangers and initial random noise.

The instantaneous acoustic field over the entire resonator length can be reconstructed from the output file of the numerical simulations that gives acoustic pressure and horizontal velocity at the entrance and exit of the active cell at all discrete times. The reconstruction is done analytically on each side of the active cell, using the d'Alembert solution, and imposing the speed of sound as a function of temperature (hot on the left resonator, and cold on the right resonator). Figure 6 shows the instantaneous acoustic pressure and horizontal velocity along the resonator in case 1, at one given instant in the saturated periodic regime. The obtained field resembles the first harmonic mode of the empty tube with closed ends, with two differences: there is a (small) discontinuity of velocity at the active cell location, and the velocity at the load end is very small but non zero.

Figure 7 shows the analogous reconstruction of instantaneous acoustic pressure and horizontal velocity along the resonator in case 2. The obtained fields resemble the fundamental mode of the empty tube with closed ends.

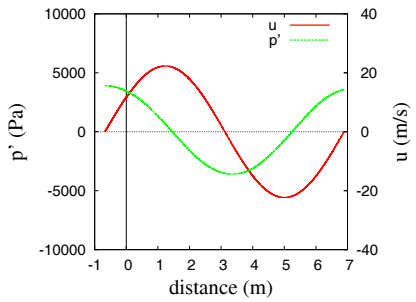

Figure 6: Instantaneous velocity and acoustic pressure over the resonator length, case 1, $f = 90$.

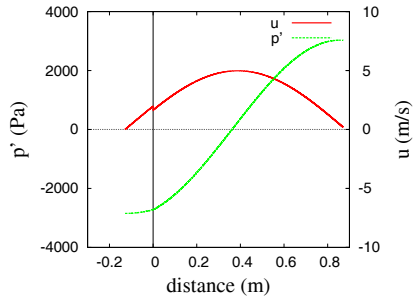

Figure 7: Instantaneous velocity and acoustic pressure over the resonator length, case 2, $f = 37.5$.

Finally, the output files can be used to estimate the acoustic power produced at a given section of the engine in the periodic regime, defined by :

$$P_{ac} = S \times \frac{1}{\tau} \int_{\tau} p' u dt, \tag{5}$$

where τ is the period of the signal and S is the section of the resonator tube. In order to smooth out numerical errors, the average value is calculated over five periods.

Similarly, the thermal power can be calculated using the instantaneous two-dimensional temperature field in the active cell, by integration over the time period of the surface integral of heat flux on the hot heat exchanger:

$$Q_h = \frac{1}{\tau} \int_{\tau} \int_{S_h} \lambda \frac{\partial T}{\partial n} dS\, dt, \tag{6}$$

where S_h is the total heat-exchanger surface, n being the outward normal vector.

Table 2: Energy balance

Case	P_{ac} (W)	Q_h (W)	η/η_C
1	66	3828	10%
2	1.685	274	1.3%

The efficiency $\eta = P_{ac}/Q_h$ can then be calculated and compared to the Carnot efficiency η_C, and results are summarized in Table 2 for both cases. The results obtained in case 1 are in agreement with experimental measures on this device. No experimental measure of efficiency is available in case 2. In both cases the efficiency is low. Improvement of the efficiency can be attempted, given the geometry and the experimental conditions, by modifying the location of the active cell or the load within the resonator. This will be the object of future work.

5 Conclusion

Using a low-Mach model and combining the numerical solution of the active cell and the analytical solution of linear acoustics, two experimental devices of standing-wave thermoacoustic engines were analyzed. One aspect of this study was the estimate of the adequate load leading to saturation and periodic operation of the engine. Several numerical strategies were tested, and showed that finding the appropriate value of the load numerically is a CPU time consuming task, which can be shorten with appropriate use of analytical approaches One fairly efficient approach consisted in choosing an initial value of the load so that there was a clear instability. Then the load was lowered until saturation was obtained, the simulation being discontinued and the value of the load changed as soon as the levels of amplification became to large. The periodic regimes were then analyzed with special focus on the unstable modes. The instantaneous acoustic field along the resonator was plotted. Finally the acoustic power and engine efficiency were estimated to be very small but comparable with experimental measurements. One of the main challenges in the development of thermoacoustic machines remains the improvement of the efficiency.

Acknowledgments

Support of the Natural Sciences and Engineering Research Council of Canada is gratefully acknowledged (L. B.). Computations were performed on the NEC-SX8 of the IDRIS-CNRS computing center, under projet No. 20599.

References

[1] N. Rott, "Damped and thermally driven acoustic oscillations in wide and narrow tubes", *Z. Angew. Math. Phys.* **20**, 230-243 (1969)

[2] G.W. Swift, "Thermoacoustic engines", *J. Acoust. Soc. Am.* **84**, 1145-1180 (1988)

[3] L. Bauwens, "Oscillating flow of a heat-conducting fluid in a narrow tube", *J. Fluid. Mech.* **324**, 135-161 (1996)

[4] G.Y. Yu, E.C. Luo, W. Dai, J.Y. Hu, "Study of nonlinear processes of a large experimental thermoacoustic-Stirling heat engine by using computational fluid dynamics", *J. Appl. Phys.* **102**, 074901-074907 (2007)

[5] J.A. Lycklama à Nijeholt, M.E.H. Tijani, S. Spoelstra, "Simulation of a traveling-wave thermoacoustic engine using Computational Fluid Dynamics", *J. Acoust. Soc. Am.* **118**, 2265-2270 (2005)

[6] O. Hireche, C. Weisman, D. Baltean-Carlès, P. Le Quéré, L. Bauwens "Low Mach number analysis of idealized thermoacoustic engines with numerical solution", *J. Acoust. Soc. Am.* **128** (6), 3438-3448 (2010)

[7] O. Hireche, C. Weisman, D. Baltean-Carlès, P. Le Quéré, M.X. François and L. Bauwens, "Numerical Model of a Thermoacoustic Engine", *Comptes rendus Mécanique* **338**, 18-23 (2010)

[8] C. Weisman, D. Baltean-Carlès, P. Le Quéré and L. Bauwens, "Modèle faible Mach et simulations numériques 2D de l'amplification d'onde thermoacoustique ", *10ème Congrès Français d'Acoustique* (2010)

[9] A. A. Atchley, H. E. Bass, T. J. Hofler, H. T. Lin, "Study of a thermoacoustic prime mover below onset of self-oscillation", *J. Acoust. Soc. Am.* **91**, 734-743 (1992)